Case Studies in Thermal Engineering 60 (2024) 104792

Contents lists available at ScienceDirect

Case Studies in Thermal Engineering

journal homepage: www.elsevier.com/locate/csite

Thermal regulation enhancement in multi-story office buildings: Integrating phase change materials into inter-floor void formers

Pouyan Mokhberi [a], Pezhman Mokhberi [b,c], Masoud Izadi [d], Mohadeseh Bagheri Nesaii [d], Wahiba Yaici [e], Federico Minelli [f,*]

[a] Civil Engineering Department, Aria University of Sciences and Sustainability, Eyvanki, Iran
[b] Architecture Group, Department of Architecture and Art, Tabari Institute of Higher Education, Babol, Iran
[c] Architecture Group, Department of Art and Architecture, Amol Institute of Higher Education, Amol, Iran
[d] Chemical Engineering Group, Engineering and Technology Faculty, University of Mazandaran, Babolsar, Iran
[e] CanmetENERGY Research Centre, Natural Resources Canada, 1 Haanel Drive, Ottawa, ON, K1A 1M1, Canada
[f] Department of Industrial Engineering, University of Naples Federico II, Naples, Italy

HIGHLIGHTS

- PCM-filled void formers (VFs) were added into the structure between office floors.
- Non-toxic bio-based PCMs were selected for better sustainability.
- Shapes of VFs, PCM types, VF locations, and PCM-insulation combinations were tested.
- 3D transient computational simulations were carried out to examine the heat flux.
- CT24W-integrated void former reduced the heat flux by up to 36.7 % for 48 h.

ARTICLE INFO

Keywords:
Thermal management
PCM
Roof
Floor
Computational fluid dynamics
Void formers

ABSTRACT

Addressing the thermal loss from building envelopes is a crucial challenge and requires the exploration of various mitigation strategies. This study employs comprehensive 3D computational fluid dynamics simulations to investigate the incorporation of various bio-based Phase Change Materials (PCMs) including CrodaTherm (CT) 19, CT21, and CT24W, within inter-floor void formers between the roof-floor boundary in multi-story office buildings to optimize energy management during inactive periods in one of the adjacent units. Aside from the PCM type, the void former shape, its placement, and the combinations of PCMs and insulating layers are examined through heat flux and solid fraction plots as well as liquid fraction contours. Results highlight the exceptional performance of CT24W-integrated void formers, achieving a remarkable 36.74 % reduction in the 48-h average heat flux in comparison with the case without void formers, and offering lower heat flux values than the scenario with insulating layers for 89.38 h (endurance time). Based on the findings, with identical PCM volumes, the semi-ellipsoid PCM-integrated void former provides 11.07 % lower heat flux and 27.56 % longer endurance time compared to the one with a spherical shape. The results underscore PCM integration as a superior strategy over standalone insulation for managing thermal loss between apartment floors.

* Corresponding author.
E-mail address: federico.minelli@unina.it (F. Minelli).

https://doi.org/10.1016/j.csite.2024.104792
Received 26 April 2024; Received in revised form 25 June 2024; Accepted 5 July 2024
Available online 7 July 2024

1. Introduction

Improving building energy efficiency is a critical effort in modern society, which can pave the way toward sustainability, efficiency, and conscientious use of resources. Buildings contribute significantly to energy consumption and carbon emissions, making it crucial to prioritize their efficiency to reduce the effects of pressing environmental issues, notably climate change [1]. By decreasing energy use in buildings, greenhouse gas emissions and carbon footprint are diminished, and a more balanced ecological setting is fostered. This not only preserves limited natural resources but also sets the stage for a sustainable future, safeguarding the planet for future generations [2]. However, this mission holds extensive importance that goes beyond environmental care. The benefits extend into the economic realm, as energy-efficient buildings offer a path to cut costs for occupants and owners [3]. Lower utility expenses, stemming from innovative technologies and designs, can lead to substantial long-term financial benefits while simultaneously enhancing the quality of life for residents. Aside from financial gains, optimizing energy consumption in buildings promotes healthier indoor environments by enhancing air quality, regulating temperature variations, and elevating overall comfort, which greatly impacts the well-being and efficiency of occupants [4].

Numerous techniques have emerged as potent tactics to attain this goal. Enhancing insulation represents one such approach [5]; it involves improving the building envelope by utilizing substances that diminish heat transfer between the inside and outside areas [6]. Upgrading windows with dual or triple-glazing [7], using insulated panels between wall layers [8], providing reflective insulation [9], and installing double-skin facades [10] or exoskeletons [11] are some of the methods to seal buildings against the weather outside, which can considerably cut down on the requirement for heating and cooling setups [12]. Another significant method involves optimizing Heating, Ventilation, and Air Conditioning (HVAC) setups [13,14]. Using high-efficiency HVAC systems, combined with intelligent thermostats and sensors, allows for exact temperature regulation and the reduction of energy waste [15,16].

The integration of renewable energies, specifically wind and solar power, into buildings has gained considerable attention [17]. Yet, the intermittent nature of solar energy, where energy production alters based on sunlight availability, poses a problem. To tackle this, inventive solutions like Phase Change Materials (PCMs) have emerged as a revolutionary tactic for enhancing energy efficiency [18]. PCMs are substances that can hold and release substantial quantities of thermal energy throughout phase change [19]. This behavior, which exploits the latent heat of phase change, finds many applications in several fields, but its slow rate impedes the advancement of these substances in some sectors. To cope with this problem, different methods of heat transfer enhancement [20] such as the use of metallic foams [21], fins [22], and nanomaterials [23,24] have been discussed by researchers. Additionally, some researchers, like Yu et al. [25] have made use of rotation-based methods to significantly enhance the melting rate, heat storage capacity, and temperature uniformity in such systems.

One of the most interesting fields of applications is in the civil sector. Integrating PCMs into building structures aids in managing temperature variations by storing extra heat during the peak sunlight hours and releasing it when necessary [26]. This feature positions PCMs as a crucial asset in addressing the irregularity of renewable energy sources like solar power. By adeptly regulating thermal fluctuations, PCMs not only help cut down on the need for typical heating and cooling systems [27] but also optimize the utilization of renewable energy. They serve as a reservoir, storing additional energy from erratic sources like solar power and redistributing it as required, ensuring a more uniform and efficient energy flow within buildings [28]. But PCMs provide also further benefits. Carbon dioxide emissions are one of the main problems of our century and PCMs may aid in the reduction of this greenhouse gas by demonstrating better performances compared to the standard insulating material. This is evidenced by studies like the one provided by Dardouri et al. [29] that focused on optimizing building envelope energy efficiency using PCMs in residential models in Tunisia. Findings highlighted substantial energy reduction (up to 76.46 %) and carbon dioxide emissions decrease by integrating PCM, emphasizing the superiority of PCM over insulation. The effectiveness of PCMs has, furthermore, been verified in different climate zones, as evidenced by the study of Ahmad and Memon [30]. They explored the synergies of PCM in building envelopes with controlled natural ventilation across 45 cities in 15 climate zones. Utilizing EnergyPlus simulations, they assessed PCM's effectiveness in reducing cooling energy consumption. The study unveiled substantial energy savings, especially in arid, warm temperate, and snowy climate zones, achieving energy savings of up to 85.3 %, when PCM and controlled ventilation were combined. These are some of the reasons that, in the last years, made the PCM research field very attractive for scientists.

In the scientific literature, several studies exist about the application of PCMs in buildings for energy efficiency enhancement purposes. To this end, PCMs are usually integrated into external building walls. In a recent study, Zhou and Razaqpur [31] devised a novel dynamic Trombe wall integrating PCM and insulation to enhance thermal efficiency. Employing a large-scale model and computational fluid dynamics (CFD), they compared this wall's thermal performance with static walls, showcasing up to 25.3 % higher energy-saving efficiencies and up to 79.8 % higher thermal efficiencies, respectively. Their findings indicated higher temperatures in the proposed wall's conditioned space during PCM discharging periods, suggesting improved thermal performance. In another work, Anter et al. [32] explored the long-term thermal behavior of building walls integrated with various PCM types and thicknesses in Egypt's climate. By using two-dimensional (2D) CFD simulations, they assessed PCM placement and types. Results indicated that PCM incorporation effectively reduces indoor heat flux, aligning internal wall temperatures with desired levels. RT-35HC exhibited superior thermal performance, with an optimal placement of 1.5 cm from both the interior and exterior wall sides. Dong et al. [33] studied PCM-integrated office building walls to optimize precooling strategies and PCM parameters. Their heat transfer model assessed energy flexibility, achieving a 69.7 % flexibility index with a 1.3 % total load reduction, saving electricity costs by 51 %. Key parameters affecting flexibility and savings were identified to be PCM thickness, density, melting point, location, and latent heat. Their recommendations included a PCM with a 25 °C melting temperature and specific placement within insulation for optimal results. From this study it can be drawn that the type of PCM can be of great importance for a specific application and, indeed, the study of PCM materials with different properties should be protracted. Not only PCM type but also its positioning within the building envelope can be of great importance for PCM integration in buildings. Positioning optimization within envelope elements has been addressed as a key field of research. Izadi et al. [34], for instance, examined Rubitherm PCMs in Iranian brick types for cold climates using CFD. They explored PCM configurations and air layer placements, highlighting RT18's 42-h endurance in reducing heat flux and RT22's 66.79 % lower average heat flux within 24 h. They noted that optimized PCM placement respecting wall thermal stratification and a combined approach of PCM and air layers show promising heat flux reduction in shelter walls. Double-layered PCM is a similar strategy used to optimize the energy behavior of this technology. Arfi et al. [35] investigated the impact of double-layer PCMs in building envelopes using numerical simulations via a finite volume approach. They varied melting temperatures and latent heat to analyze heat loss during the charging cycle. Results highlight that the outer layer's melting temperature significantly controls heat loss, showing a rise of 18 % in excess heat for one of the cases compared to the reference case. Moreover, the research underlines the interplay between PCM layers, showcasing high solid fractions when the inner layer's melting temperature is higher or the latent heat is lower than the outer layer.

From the outcomes of the reported studies, it can be stated that studying different typologies and combinations of PCMs and their positioning concerning envelope structures is very important for applications in this sector. In this regard, the study of Muzhanje and Hassan [36] delved into optimizing PCMs in diverse encapsulation shapes, aiming to redefine building thermal control. Through exhaustive thermal analysis and modeling, they explore different PCMs, integrating with various nanoparticles. They focused on enhancing heat transfer specifically for buildings, emphasizing free heating in cold climates. The findings highlighted up to 41 % faster melting and solidification in rectangular capsules. Li et al. [37] numerically and experimentally analyzed the thermal behavior of a concrete wall incorporating PCMs in different climatic conditions across China. Encapsulated in polyethylene shells, PCMs were integrated into the concrete to form a PCM-concrete layer, and simulations were conducted for various PCM positions within the wall. Findings regarding PCM position optimization emphasized that during winters with moderate temperatures, positioning the PCM near the outer wall leads to the best results; however, the placement may vary based on ambient temperature. Neither of these two studies, however, addresses PCM encapsulation in roofs or floors, which could provide further benefits to the energy efficiency of the analyzed building.

The applications of PCMs on floors and ceilings are relatively rare to find. An application to building floors is found in the study of Jeong et al. [38], where a carbon-based PCM was developed by combining n-eicosane and activated carbon in a PVC container for heat storage in buildings. They evaluated the thermal properties and performance of the PCM in a dry floor heating system, observing its superior heat transfer over pure n-eicosane due to its higher thermal conductivity. The PCM showed a time-lag effect during heating and free cooling, reducing energy consumption by 77.3 % compared to wet floor heating. Their analysis highlighted the potential for PCM-based systems, emphasizing the need to enhance thermal conductivity in PCM container materials for improved efficiency.

For this purpose, the encapsulation of PCMs in void formers could be an interesting research field, leading to major improvements in the thermal behavior of buildings. Void formers are innovative components used in building construction primarily to reduce the dead load of concrete slabs while maintaining their structural integrity. They are hollow or voided structures that are placed within concrete slabs during construction and are usually made from materials like plastic. Depending on the specific application they come in different shapes and sizes. Since these devices are easily installed, they can accelerate the construction process and reduce the use of raw materials and energy consumption in buildings. Additionally, these components can elevate the flexibility of the building design in terms of architecture since they allow for larger open spaces due to the reduction of weight.

As was covered in the literature review section, numerous approaches have been taken by researchers to eliminate the considerable heat loss from building envelopes, most of them concentrating on the use of PCM integration within windows or walls. The few studies that have examined the use of PCM incorporation within roofs or floors have focused on single-story buildings, having no connection or heat transfer with the neighboring units. This research explores the integration of PCM materials within the void formers between floors in apartment buildings. Notably, the current research tries to fill in the unexplored research gap regarding the use of various bio-based PCMs (CrodaTherm 19, CrodaTherm 21, and CrodaTherm 24W) within these inter-floor void formers with different shapes. For this purpose, unlike many studies in this field, the research uses three-dimensional (3D) simulations to examine the heat transfer behavior with the aim of enhancing building energy management during the time that the neighboring office units on different floors and their HVAC systems are not active. The importance lies in the fact that the working times of all office buildings are not identical, and some of them might be active during the weekends. Through a comprehensive analysis of diverse PCM types, PCM layer positions within the void former, different PCM layer combinations within the void former, and the combination of PCM and Styrofoam layers, this study addresses a critical aspect of building energy management, shedding light on effective thermal regulation between apartment floors.

2. Physical model

This research tries to reduce the heat loss between two consecutive floors in an office apartment building to reduce the reliance on heating devices for a limited time when one of these two offices and its HVAC system is not active. To do so, a 337.5 mm × 337.5 mm section from the floor of the top unit and the roof of the bottom unit is separated as the test zone and modeled using the numerical method within a commercial CFD software package. Fig. 1a exhibits the layers in this section and their thickness. As can be observed, these layers from top to bottom are made of ceramic tile (15 mm), concrete (10 mm), foam concrete (50 mm), reinforced concrete (320 mm), and gypsum plaster (15 mm). It is necessary to mention that the void formers are placed within the reinforced concrete layer (in the middle for most cases), and the PCM or Styrofoam has been incorporated into the cavity within the void formers. The size and shapes of the void formers, which were inspired by the COBIAX ® economic-line (EL) and slim-line (SL) models, have been illustrated in Fig. 1b. Additionally, Fig. 1c illustrates the position of the computational domain and void former within the building body.

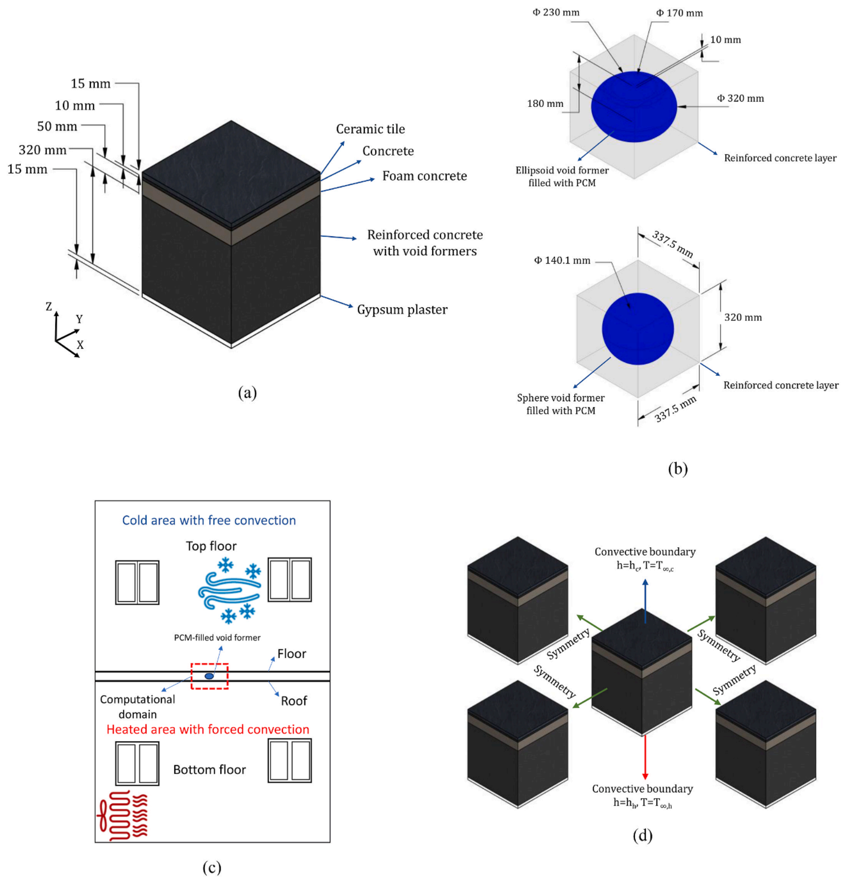

Fig. 1. The geometric specifications of the examined section: (a) the complete domain, (b) the void formers, (c) the location of the computational domain, and (d) the boundary conditions.

To ensure that the amount of the incorporated PCM does not vary with the shape of the void formers, both these containers were designed in such a way that they have the same inner volumes (11.50 L). Therefore, the PCM volumes are identical with both the spherical and semi-ellipsoid shapes of void formers.

Table 1 tabulates the thermophysical characteristics of the materials used in simulations.

It is necessary to mention that since the PCMs and Styrofoam have densities up to 62.15 % and 98.87 % lower than reinforced concrete, their integration within the void formers does not interfere with the main objective of using these components within the building roofs, which is to reduce the dead load of the concrete slabs. Also, as provided in Table 2, to assess the impact of the investigated variables, the subsequent scenarios were analyzed.

Table 1
The values applied for the thermophysical properties [39,40].

Materials		Property						
Type	Name	ρ [kg·m^{-3}]	C_p [J·kg^{-1}·K^{-1}]	k [W·m^{-1}·K^{-1}]	h_{sf} [J·kg^{-1}]	T_{sf} [K]	μ [Pa·s]	β [K^{-1}]
Construction	Ceramic Tile	2600	900	2.5	–	–	–	–
	Concrete	2100	840	1.4	–	–	–	–
	Foam Concrete	800	1000	0.3	–	–	–	–
	Gypsum Plaster	1680	1085	0.22	–	–	–	–
	Reinforced Concrete	2300	1000	2.3	–	–	–	–
Insulation	Styrofoam	26	1200	0.037	–	–	–	–
PCM	CrodaTherm 19	880.5	2150	0.195	176000	292	0.016	0.00480
	CrodaTherm 21	870.5	2100	0.165	190000	294	0.020	0.00200
	CrodaTherm 24W	874.5	2950	0.19	182000	297	0.021	0.00375

Table 2
The studied cases.

Parameter	Case	Variety of PCMs/Materials	Void Former Type	Void Former Position	Arrangement of layers	
					Top	Bottom
Base	1	No Void Former	–	–	Reinforced Concrete	
PCM Type	2	Single PCM	Ellipsoid	Middle	CT19 PCM	
	3				CT21 PCM	
	4				CT24W PCM	
Void Former Type	4	Single PCM	Ellipsoid	Middle	CT24W PCM	
	5		Spherical			
Void Former Placement	4	Single PCM	Ellipsoid	Middle	CT24W PCM	
	6			50 mm higher		
	7			50 mm lower		
Combination of PCMs	8	Combination of PCMs	Ellipsoid	Middle	CT19 PCM	CT24W PCM
	9				CT24W PCM	CT19 PCM
Combination of PCM and Insulation	10	Combination of PCM and Styrofoam	Ellipsoid	Middle	ST	CT24W PCM
	11				CT24W PCM	ST
Base	12	Insulation Only	Ellipsoid	Middle	ST	

In which, ST indicates Styrofoam.

3. Methodology

3.1. Assumptions

To simulate the problem within the computational domain, several assumptions were applied. These assumptions are listed below:

- The models used are transient and 3D.
- Free stream velocities and temperatures remain constant throughout the simulations.
- The materials utilized in the research are assumed to possess isotropic and homogeneous properties.
- Thermal contact resistance amidst the roof/floor layers is disregarded since the temperature difference is not significant [34].
- Supercooling is disregarded throughout the solidification process.
- The PCM employs the Boussinesq model to account for the impact of natural convection.
- An initial temperature of 297.1 K is used for all zones.
- To examine the worst case with the highest heating loss, and considering the fact that due to the buoyancy effects, hot air goes near the roof and cold air remains near the floor, the active office unit with heating was considered to be located on the bottom floor, and the top floor was chosen to be inactive and without heating throughout the simulation time.
- To maximize the heat transfer and challenge the advantages of PCM-filled void former insertion, the winter condition with the highest logical temperature difference possible was considered for the simulations.

3.2. Equations

Due to the absence of fluid flow in the solid layers, including gypsum plaster, Styrofoam, reinforced concrete, foam concrete, and ceramic tile, there are no continuity and momentum equations, and the energy equation is written in the form of the transient 3D thermal conduction:

$$\frac{\partial T}{\partial t} = \frac{k}{\rho C_p}\nabla^2 T \tag{1}$$

However, the continuity and momentum equations are solved for the PCM region [12]:

$$\nabla \cdot V = 0 \tag{2}$$

$$\frac{\partial V}{\partial t} + V \cdot \nabla V = \frac{1}{\rho}\left(-\nabla P + \mu \nabla^2 V + \rho\beta\left(T - T_0\right)\right) - \frac{(1-\varphi)^2}{\varphi^3} C_m V \tag{3}$$

where, the mushy zone constant (C_m) was chosen equal to 10^5 (kg/m^3·s) based on previous studies [41]. It should be noted that the Boussinesq approximation is employed to account for the influence of natural convection within the PCM layers. Also, the energy equation for the PCM region is written as [19]:

$$\frac{\partial e_{\text{sensible}}}{\partial t} + \frac{\partial e_{\text{latent}}}{\partial t} + \nabla \cdot \left(V e_{\text{sensible}}\right) = \nabla \cdot \left(\frac{k}{\rho c_p}\nabla e_{\text{sensible}}\right) \tag{4}$$

$$e_{\text{sensible}} = e_0 + \int_{T_0}^{T} c_p dT = e_0 + c_p \int_{T_0}^{T} dT \quad (5)$$

$$e_{\text{latent}} = \sum_{i=1}^{n} \lambda_i e_{fusion} \quad (6)$$

$$\lambda = \left\{ \begin{array}{c} \frac{e_{\text{latent}}}{e_{fusion}} = 0 \text{ if } T \le T_{\text{solid}} \\ \frac{e_{\text{latent}}}{e_{\text{fusion}}} = \frac{T - T_{\text{s}}}{T_{\text{l}} - T_{\text{s}}} \text{ if } T_{\text{solid}} < T < T_{\text{liquid}} \\ \frac{e_{\text{latent}}}{e_{fusion}} = 1 \text{ if } T \ge T_{\text{liquid}} \end{array} \right\} \quad (7)$$

The above equations made use of the enthalpy porosity approach, which considers the phase change process by modeling it through porosity. Based on this approach, the term solid fraction (φ) varies between 0 and 1, showing complete liquid and complete solid states for each cell, respectively.

To assess the time-dependent heat flux ($\dot{W}$) [W/m^2], the roof of the bottom floor, or in simpler words, the bottom surface of the computational domain ($T_{surf,\ r}$) was chosen as the basis [42], and the value was measured based on the convection coefficient (h_h) and free stream temperature of the hot side ($T_{\infty,\text{h}}$):

$$\dot{W} = h_h \left(T_{\infty,\text{h}} - T_{sur,\text{r}}\ (t) \right) \quad (8)$$

To determine the energy consumption per unit of the area [W·hr/m^2 or J/m^2] the above equation can be integrated over a specific period [42]:

$$\dot{W} = \int_{t=0}^{t=p} \dot{W}(t)\, dt \quad (9)$$

According to the above value, the average heat flux throughout a specific period can be written as [42]:

$$\dot{W}_{Avg} = \frac{\int_{t=0}^{t=p} \dot{W}(t)\, dt}{\int_{t=0}^{t=p} tdt} = \frac{W}{p} \quad (10)$$

3.3. Boundary conditions

The boundary conditions used for the problem can be observed in Fig. 1d. These conditions will be clarified through the equations listed below:

A coupled condition is applied on the interface between the vertical layers (the layers of the roof and the floor):

$$-k_i \frac{\partial T_i}{\partial n} = -k_j \frac{\partial T_j}{\partial n} \quad (11)$$

In which n refers to all cartesian directions, x, y, and z, and i or j denote a pair of neighboring elements across distinct layers. By noting that the center point of the bottom surface was located on the origin (x, y, and z = 0), the horizontal border of the geometry was given a symmetry boundary condition:

$$-k \frac{\partial T}{\partial x}\bigg|_{y=\pm 500\ mm} = -k \frac{\partial T}{\partial y}\bigg|_{x=\pm 500\ mm} = 0 \quad (12)$$

Moreover, the top and bottom surfaces were given a convection boundary [43]:

$$-k \frac{\partial T}{\partial z}\bigg|_{z=0\ mm} = h_{\text{c}} \left(T_{\infty,\text{h}} - T_{surf,\text{r}}\ (t) \right) \quad (13)$$

$$-k \frac{\partial T}{\partial z}\bigg|_{z=410\ mm} = h_{\text{h}} \left(T_{surf,\text{f}}\ (t) - T_{\infty,\text{c}} \right) \quad (14)$$

In the above equations, $T_{surf,\ r}$ is employed to express the surface temperature of the bottom layer in the computational domain (the roof of the bottom floor), and $T_{surf,\ f}$ shows the surface temperature of the top layer in the computational domain (the floor of the top floor). Additionally, $T_{\infty,h}$ and $T_{\infty,c}$ represent the free stream temperatures in the bottom and top floors, respectively. Also, by considering that the bottom floor has forced convection because of the active fan coil heating unit (FCU), and the top floor relies solely on natural convection and relatively mild airflow in the absence of HVAC devices, the values of $h_h = 15$ W/m^2·K and $h_c = 10$ W/m^2·K were selected for these two horizontal surfaces which are in the ranges reported in the literature and standards [34,44].

3.4. Numerical approach

CFD simulations were done in a CFD software package using the finite volume approach in unsteady mode. Each time step was permitted a hundred iterations, with energy, continuity, and velocity residuals meeting a convergence criterion of 10^{-6}, 10^{-4}, and 10^{-4}, respectively. Moreover, for pressure, momentum, and energy discretization, the PRESTO, QUICK, and QUICK, schemes were utilized.

4. Method verification

4.1. Validation

To test the accuracy of the model developed for the problem, it was essential to test the model with an approximately similar experimental case and make a comparison between the numerical results and the experimental ones. For this purpose, the PCM-incorporated wall analyzed in the research of Hasan et al. [45] was simulated. Here are the specifications of this experimental work: polystyrene sheet with a thickness of 20 mm was used to build a 400 mm × 400 mm × 400 mm cubic chamber, the front of which was enveloped with a polystyrene layer (10 mm), a Rubitherm RT42 PCM layer (50 mm), and a concrete wall (25 mm), an air layer (100 mm) and another concrete wall (25 mm). Thermocouples were then used to collect temperature values from the front of the first wall (inner surface) and the back of the second wall (outer surface). Fig. 2a and b present the comparison of the acquired numerical values for these temperatures and the experimental values reported in the research of Hasan et al. [45]. According to the figure, the acquired numerical values align closely with experimental ones, having a maximum deviation of 4.38 and 4.71 for inner and outer surfaces, respectively.

4.2. Independence analysis

To verify the precision of the numerical model, grid and time-step size sensitivity analyses were conducted for Case 4 (semi-ellipsoid void former located in the middle and filled with CT-24 PCM), and the predicted values were obtained as plots in Fig. 3. According to the fact that from the four tested time-step sizes, the case with a time-step size of 1 s provides results significantly close to the one with a smaller time-step size, a time-step size of 1 s was selected for the tests. On the other hand, since it was found that the mesh network with 1,650,000 cells provides heat flux values and a trend that is indistinguishable from those with a finer mesh network, a network with this number of cells (as illustrated in Fig. 3c) was chosen for the remaining tests. These values provide a well-balanced model in terms of precision and computational cost.

5. Results and discussions

In this section, the influence of various parameters including the type of PCM in the inter-floor void formers, the shape of these void formers, their placement within the reinforced concrete layer, the combination of different PCMs, and their combination with insulating layers have been extensively examined through a series of complex 3D numerical simulations and have been discussed. Different parameters such as the changes in heat flux, the solid fraction, and liquid fraction contours were acquired and used for the analyses.

5.1. Various PCM types

In this part, different types of PCMs are integrated into the void formers between floors, and the effects of these PCMs are evaluated on the changes of heat flux and solid fraction plots, as well as the liquid fraction contours. Fig. 4 presents the heat flux changes as well as the PCM solid fraction progression in both, the top, and bottom halves of the void former. It is evident that among the cases

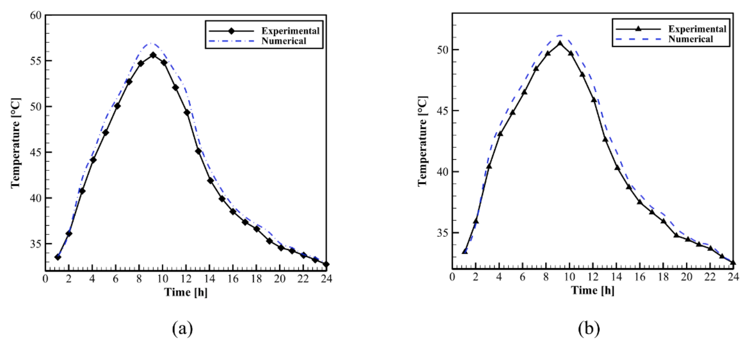

Fig. 2. Validity test of the model with experimental data [45] at (a) the outer, and (b) inner surfaces.

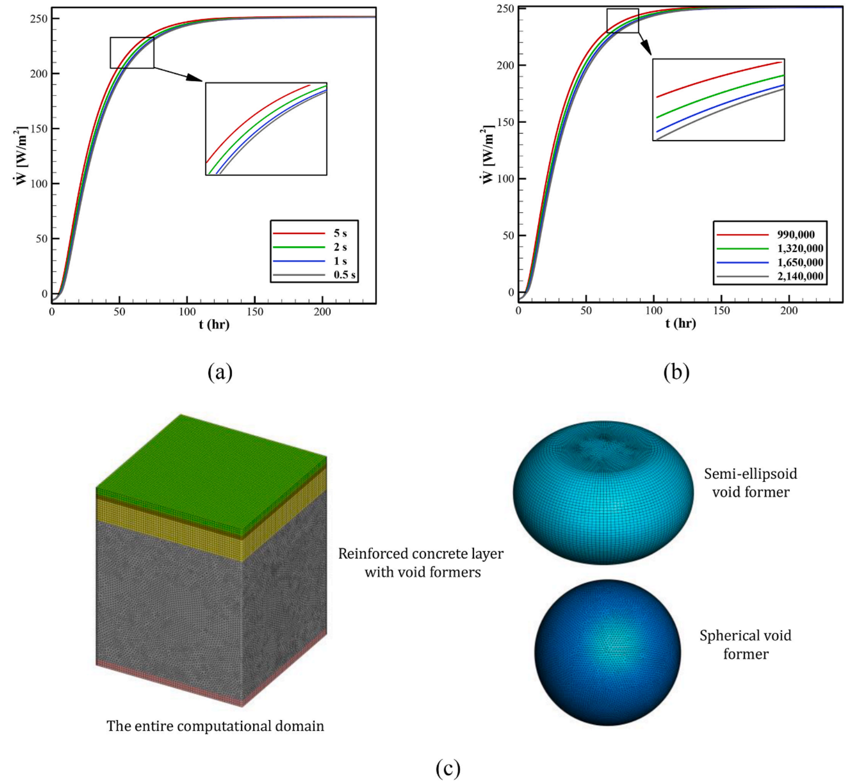

Fig. 3. The plots of (a) time-step size, and (b) mesh size analysis tests, as well as (c) the selected generated mesh network.

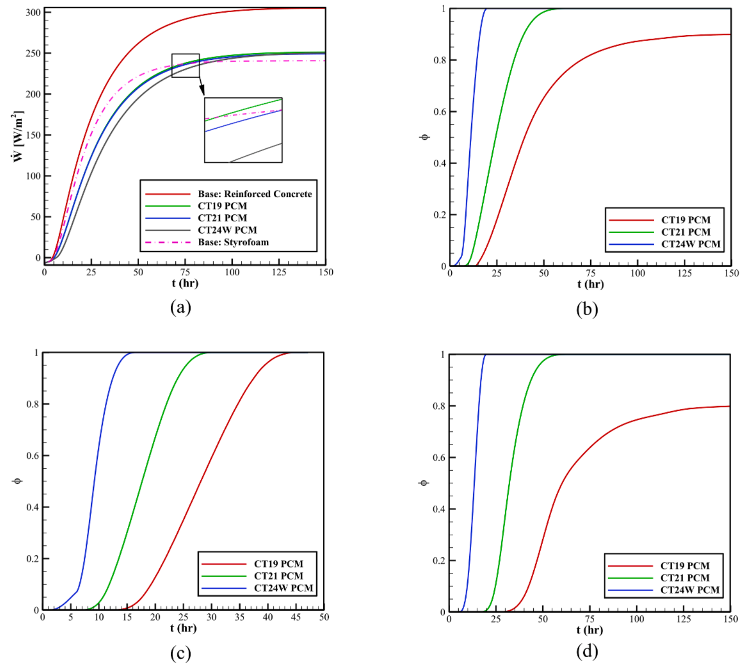

Fig. 4. The alternations of (a) heat flux, (b) averaged total solid fraction, (c) solid fraction in the top and (d) bottom halves of the void formers integrated with various PCMs.

with various PCM types, CT24W achieves the fastest solidification time due to its lower latent heat of 182,000 J/kg and a phase change temperature of 297 K, which is closer to the system's initialization temperature. These properties allow CT24W to solidify more quickly compared to other PCMs, despite having a higher latent heat than CT19, whose phase change temperature is too low to reach complete solidification before the system stabilizes.

To be able to comprehend the impact of PCM encapsulation on the reduction of heat flux values, two benchmark cases with reinforced concrete and Styrofoam filling were also considered for the comparison. As can be observed in Fig. 4a, the use of insulation or PCM layers can significantly diminish the heat flux values over the whole simulation time. As could be expected, because of the higher thermal conductivity of PCMs than that of the insulation layer, after a long time, the case with Styrofoam layer has the capacity to offer reduced heat flux measurements compared to the ones with PCM integration; however, it is important to note that over a considerable amount of time, the ones with PCM filling can keep the heat flux values lower. To be able to quantitively discuss this, similar to the previous work of Izadi et al. [34], a factor known as the endurance time was delineated which refers to the time that the cases with PCM integration keep the thermal performance better (or the heat flux lower) than the case with solely the insulation layer. The values of this parameter, as well as the mean heat flux measurements, are provided in Table 3.

According to this table, compared to the case without a void former, the cases with CT19, CT21, and CT24W PCM integrations can reduce the 48-h average heat flux by 26.22 %, 26.48 %, and 36.74 %, respectively, while the case with Styrofoam insulation offers only a 13.51 % improvement over the case without a void former. By considering the endurance time of these PCMs, it is conspicuous that the cases with these PCMs could outperform the case with Styrofoam layer over the first 73.39, 78.04, and 89.38 h, meaning that these cases can retain the heat flux values lower for these periods which are much longer than the 48-h time required for this problem. Based on this, among the examined cases in this section, the CT24W PCM integration offers the best performance for the intended application. It is important to note that the endurance time of cases with PCM is higher than their solidification time due to the transient nature of heat transfer, where the time needed for cold to penetrate the body must be considered. Even after the PCM solidifies, the system continues to lose heat, causing the temperature to drop gradually. The endurance time thus reflects the total duration during which the PCM can maintain thermal regulation, not just the solidification period.

Fig. 4b, c, and 4d illustrate the changes in solid fraction values over time in the entire container, the top half, and the bottom half, respectively. As can be observed, the solidification rate of the PCMs with higher phase change temperatures is higher. The complete phase change of CT24W and CT21 PCM layers takes 18.51 and 51.16 h while the case with CT19 PCM reaches a steady state condition without completely freezing. By taking a closer look at the different solid fraction changes in the top and bottom halves of the container, it is evident that the top half solidifies in the cases with all PCMs because this half is closer to the cold boundary; nevertheless, the complete solidification does occur in the bottom half of the container in the case with CT19 PCM. The liquid fraction contours depicted in Fig. 5 offer a clearer observation regarding the progression of the solidification front.

According to this figure, it can be observed that the case with CT19 PCM integration suffers from the slow phase change process, and over the entire 48-h period, the solidification process is not complete in the bottom half of the void former. Also, the solidification front in all cases is not uniform in the top and bottom halves which is mainly due to the difference in the top and bottom boundary conditions of the computational domain, and partly due to the insignificant influence of natural convection in the enclosure; however, similar to the observations of Afsharpanah et al. [13,14], the impact of this heat transfer mechanism is minimal, since the solidification process relies mostly on thermal conduction as the main heat transfer mechanism.

5.2. Different shapes of void formers

In this section, various shapes of PCM-integrated void formers are tested in the inter-floor roofs, and their effects on the changes of heat flux and solid fraction plots, as well as solid fraction contours, are discussed. Fig. 6 presents the alternations of the heat flux and solid fraction values throughout the simulations with various shapes of void formers. As illustrated, the semi-ellipsoid shape of the PCM-integrated void former provides the lowest heat flux over the simulation time. Based on the values tabulated in Table 4, in the first 24 and 48 h, compared to the case with the spherical-shaped void former, the semi-ellipsoid one presents heat flux values 7.42 % and 11.07 % lower, respectively. Additionally, even though the volume of the PCM with these two container shapes is the same, the PCM-integrated semi-ellipsoid container offers 27.56 % longer endurance time, although both shapes provide endurance times that exceed the 48 h intended for the application (the weekend) and are not necessary. In other words, both of these shapes can retain the heat flux measurement less than the case with insulation over a long period; a period longer than the 48 h that is needed for the office on the top floor to start operating and turning on the heating system.

Considering the solid fraction changes in Fig. 6b, it can be noticed that for most of the simulation time, the solidification process is faster in the case with a PCM-integrated spherical container. The reason can be sought in the fact that since these containers have

Table 3
The influence of PCM type on the average heat flux and the endurance time values.

Case	Average Heat Flux (W/m^2)		Endurance time (hr)
	24-h	48-h	
Base: Reinforced Concrete	213.87	144.17	–
CT19 PCM	168.20	106.36	73.39
CT21 PCM	167.21	105.98	78.04
CT24W PCM	156.23	91.20	89.38
Base: Styrofoam	178.47	124.69	–

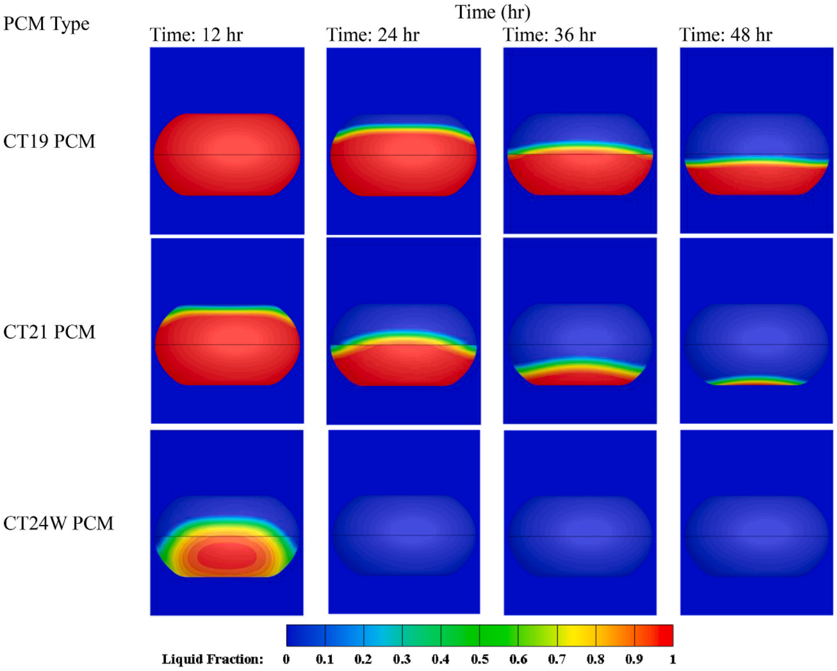

Fig. 5. The advancement of the solidification front in void formers with various PCM types over time.

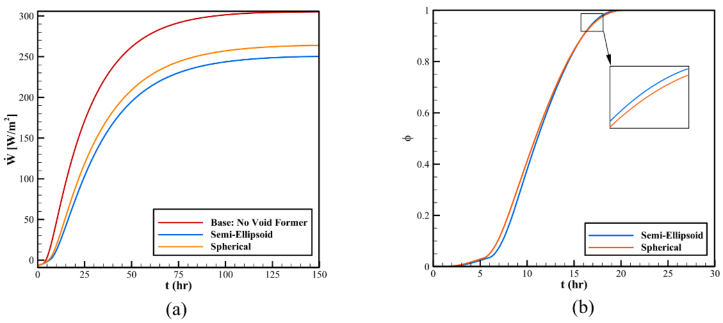

Fig. 6. The changes of (a) heat flux, and (b) averaged total solid fraction with various PCM-integrated void formers.

Table 4
The influence of PCM-integrated void former shapes on the average heat flux and the endurance time values.

Case	Average Heat Flux (W/m^2)		Endurance time (hr)
	24-h	48-h	
Base: No Void Former	213.87	144.17	–
Semi-Ellipsoid	156.23	91.20	89.38
Spherical	168.75	102.55	64.74

identical volumes, the spherical container has to be less wide but taller. This makes the PCM in the container closer to the cold front and accelerates the solidification process for the early stages. Nevertheless, near the end of the process, the progression of the solid fraction values becomes more similar for the cases with semi-ellipsoid and spherical shapes of void formers, so that the complete solidification time of the PCM in these cases is 18.5 and 18.83 h, respectively (less than 1.76 % of difference). The advancement of the solid front can be better observed in the liquid fraction contours of Fig. 7.

As illustrated in the contours, the advancement of the phase-change front is relatively similar, and while the shapes of the solidification front are influenced by the shape, the process advancement is not significantly altered.

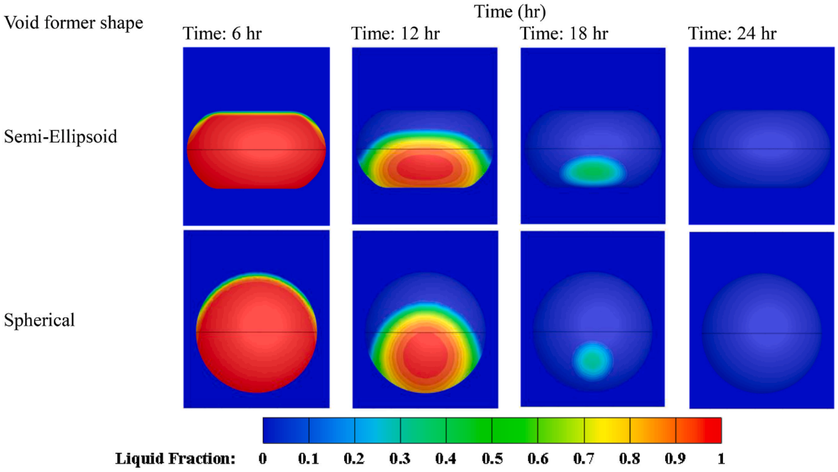

Fig. 7. The advancement of the solidification front in void formers with different PCM-integrated void former shapes over time.

5.3. Placement of PCM-filled void formers

In this part, efforts were made to examine the impacts of PCM-integrated void former placement on the alternations in heat flux and solid fraction measurements. Fig. 8 shows the influence of this parameter on the heat flux and solid fraction changes over the simulation time. As it can be observed, moving the void former slightly upward or downward does not lead to considerable changes in the heat flux, and at least in plots there is no meaningful pattern; however, by taking a close look at the values for the first 24 and 48 h of the simulation, it is evident that moving the PCM-integrated container slightly closer to the cold boundary (the top floor), the average heat flux values are slightly improved. Comparing the cases with PCM-integrated void formers, it is evident that moving the void former slightly higher (+50 mm in the Z direction) can reduce the 48-h average heat flux by 2.34 %; however, moving it slightly lower (−50 mm in the Z direction) elevates this parameter by 5.22 %. The results of the endurance time do not follow this pattern, as moving the PCM-integrated void former upward and downward slightly worsens the endurance time (by 2.91 % and 5.91 %, respectively). It is also noticed that moving the void former upward leads to higher solidification rates, which can be explained that this way the container would approach the cold side and reach complete solidification slightly faster. Additionally, the changes in the endurance time and average heat flux values for these cases with different void former positions can be found in Table 5.

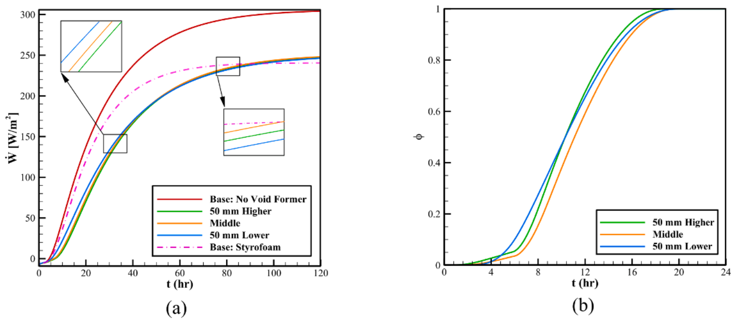

Fig. 8. The changes of (a) heat flux, and (b) averaged total solid fraction with different PCM-integrated void former positions.

Table 5
The impact of the PCM-integrated void former placement on the average heat flux and the endurance time values.

Case	Average Heat Flux (W/m^2)		Endurance time (hr)
	24-h	48-h	
Base: No Void Former	213.87	144.17	–
50 mm Higher	154.68	89.06	92.06
Middle	156.23	91.20	89.38
50 mm Lower	157.94	96.23	95.00
Base: Styrofoam	178.47	124.69	–

5.4. Combination of PCMs

This section focuses on testing various combinations of PCM combinations within the void former. The influence of these combinations is assessed by observing the heat flux values and changes of the solid fraction in the entire enclosure, and the top and bottom halves separately. These values are provided in the plots of Fig. 9.

As it can be noticed, even though the case with the CT24W PCM in both the top and bottom layers still provides the lowest heat flux values in the entire process, the cases in which the combination of CT19 and CT24W PCMs are used offer better results than the case with only the CT19 PCM. Between the cases with combinations of CT24W and CT19 PCMs, the one with CT24W PCM at the top and the CT19 PCM at the bottom provides a lower heat flux value, so that, compared to the one that has the opposite order, it offers 2.71 and 6.59 % enhanced insulating capability over the first 24 and 48 h, respectively. The same superiority is noticed for the endurance time as well (by up to 4.02 %). In other words, placing the PCM with a higher solidification temperature near the cold surface and selecting the one with a lower solidification temperature near the hot wall results in a better result regarding the heat flux reduction and endurance time extension. The other important point is the changes in the solid fraction values. As can be observed in Fig. 9b, c, and 9d, while the solidification process completes in the top half for all the configurations, the solidification cannot be completed in the cases where the bottom half is filled with the CT19 PCM. This is because the bottom half is near the hot side and the temperature does not drop as significantly as it should to make this half solidify completely. Moreover, the changes in the endurance time and average heat flux values for the cases with various PCM combinations can be found in Table 6.

5.5. Combination of PCM and insulating layers

This part of the paper concentrates on discussing the impact of combining PCMs and insulating layers. Fig. 10 shows the alternations of the heat flux and solid fraction measurements with various combinations of PCM and Styrofoam layers. As it can be noticed, for a considerable amount of time, the case with only CT24W PCM integration provides the lowest heat flux values; however, as should be expected, since this PCM has a higher thermal conductivity than Styrofoam, eventually after reaching the steady state, it

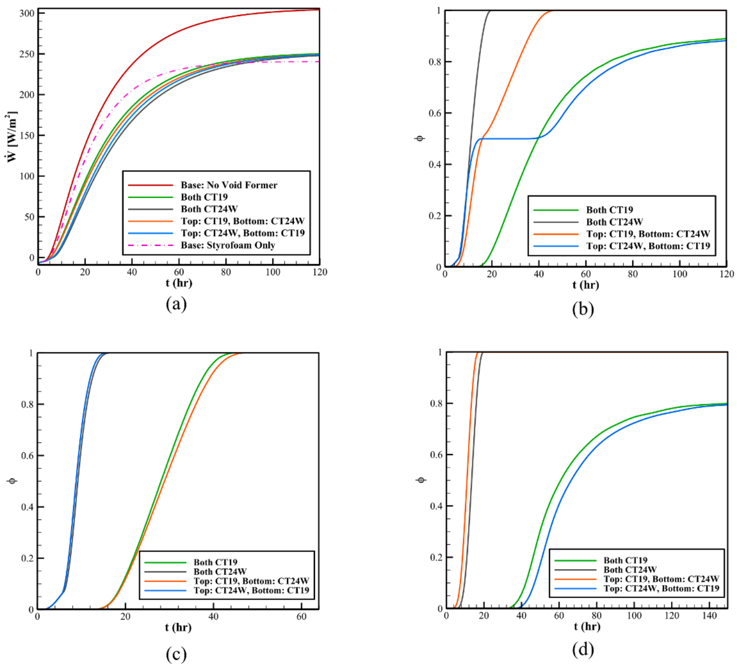

Fig. 9. The changes of (a) heat flux, (b) averaged total solid fraction, (c) solid fraction in the top and (d) bottom halves of the void formers integrated with various combinations of PCMs.

Table 6
The effects of various PCM combinations on the average heat flux and the endurance time values.

Case	Average Heat Flux (W/m^2)		Endurance time (hr)
	24-h	48-h	
Both CT19	168.20	106.36	73.39
Both CT24W	156.23	91.20	89.38
Top: CT19, Bottom: CT24W	164.80	102.59	79.90
Top: CT24W, Bottom: CT19	160.33	95.83	83.25

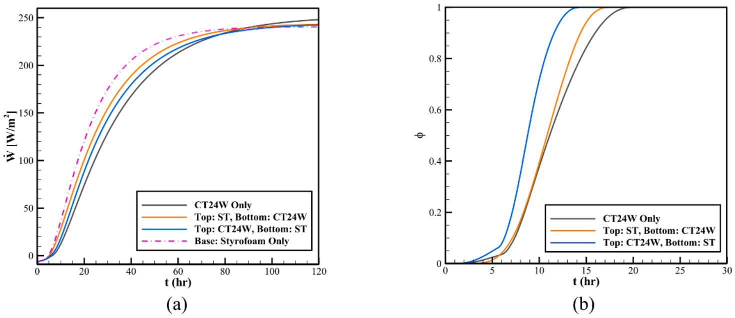

Fig. 10. The changes of (a) heat flux, and (b) averaged total solid fraction with void formers integrated with various combinations of Styrofoam and PCM layers.

shows slightly higher heat flux values. According to the plot, comparing the cases with combinations of Styrofoam and PCM layers, the one that places the PCM layer near the hot side and the insulating layer near the cold side provides a better result. Based on the predicted values from Table 7, over the first 24 and 48 h, the order mentioned results in mean heat flux measurements that are 3.93 and 8.16 % less compared to those of the opposite order, respectively. On the other hand, employing the opposite order by inserting the PCM layer in the vicinity of the cold side and inserting the Styrofoam layer in near the hot side offers a 10.93 % higher endurance time, which would not be necessary for the intended application. Thus, regarding the combination of PCMs and insulation layers, it is better to move the PCM layer near the thermally-regulated side.

6. Conclusions

In this research, it was tried to examine the influence of using PCM-integrated void formers within the inter-floor roof of apartment offices to reduce the thermal loss between the floors when one of the offices and its heating system is not active. Different parameters such as various bio-based PCMs from the CrodaTherm™ company (including CT19, CT22, and CT24W), various void former shapes (spherical and semi-ellipsoid), different PCM-integrated void former placements, and different combinations of PCMs and insulating layers were tested. Here are the main findings:

- Compared to the case without a void former, using a CT24W-integrated void former can reduce the 48-h average heat flux between floors by 36.74 %, which is considerably higher than the improvement that can be obtained by Styrofoam insulating layers by up to 26.85 %. This type of PCM outperforms the CT19 and CT22 PCMs in terms of the mean heat flux and endurance time measurements.
- The use of CT24W PCM integration can offer heat flux measurements less than the case with only insulating layers for up to 89.38 h (endurance time).
- Using an identical volume of PCM in void formers with spherical or semi-ellipsoid shapes reveals that by using a semi-ellipsoid shape instead of the spherical one, the 48-h average heat flux value can be reduced by up to 11.07 %. Also, this shape provides a 27.56 % longer endurance time. Therefore, the semi-ellipsoid shape is more recommended for buildings.
- Moving the PCM-integrated void former slightly upward (closer to the cold boundary) can decrease the 48-h average heat flux by 2.34 %, and moving it downward can increase this parameter by 5.22 %. Regardless of this, moving the void former from the center worsens the endurance time.
- Using the combination of PCMs do not offer any improvement over the case with the best type of PCM (CT24W); however, in case of using a combination of PCMs, not obeying the thermal stratification of the construction layers by placing the PCM with the higher solidification temperature near the cold side and placing the one with the lower phase-change temperature near the hot side results in better endurance time and average heat flux values compared to those of the case with the opposite order.
- The combination of PCM and insulating layers works more efficiently when the PCM is inserted near the hot side (active office) and the insulating layer is placed near the cold side (inactive office). However, still, the case with PCM integration provides better results than this combination.

Table 7
The effects of various PCM and insulation layer combinations on the average heat flux and endurance time values.

Case	Average Heat Flux (W/m^2)		Endurance time (hr)
	24-h	48-h	
CT24W Only	156.23	91.20	89.38
Top: ST, Bottom: CT24W	169.10	110.48	89.82
Top: CT24W, Bottom: ST	162.44	101.46	100.85
Base: Styrofoam	178.47	124.69	–

Future work could focus on integrating PCMs with other building envelope materials, studying their long-term durability, and enhancing dynamic thermal modeling for various climatic conditions and seasonal changes. Additionally, investigating adaptive PCM systems with real-time optimization, performing comprehensive cost-benefit analyses, and assessing health and safety aspects will further advance the practical application of PCMs in building thermal regulation.

CRediT authorship contribution statement

Pouyan Mokhberi: Writing – review & editing, Software, Resources, Methodology, Data curation. **Pezhman Mokhberi:** Writing – original draft, Visualization, Investigation, Formal analysis, Data curation. **Masoud Izadi:** Writing – original draft, Validation, Software, Methodology, Investigation, Conceptualization. **Mohadeseh Bagheri Nesaii:** Visualization, Software, Investigation, Data curation. **Wahiba Yaici:** Writing – review & editing, Supervision, Resources, Project administration. **Federico Minelli:** Writing – review & editing, Validation, Supervision, Resources, Funding acquisition.

Declaration of competing interest

The authors declare that they have no known competing financial interests or personal relationships that could have appeared to influence the work reported in this paper.

Data availability

Data will be made available on request.

References

[1] F. Minelli, I. Ciriello, F. Minichiello, D. D'Agostino, From net zero energy buildings to an energy sharing model - the role of NZEBs in renewable energy communities, Renew. Energy 223 (2024) 120110, https://doi.org/10.1016/j.renene.2024.120110.

[2] A. Levesque, R.C. Pietzcker, G. Luderer, Halving energy demand from buildings: the impact of low consumption practices, Technol. Forecast. Soc. Change 146 (2019) 253–266, https://doi.org/10.1016/j.techfore.2019.04.025.

[3] A.H. Al-Badi, S.N. Al-Saadi, Toward energy-efficient buildings in Oman, Int. J. Sustain. Energy 39 (5) (2020) 412–433, https://doi.org/10.1080/14786451.2019.1685521.

[4] D. D'Agostino, F. Minelli, F. Minichiello, M. Musella, Improving the indoor air quality of office buildings in the post-pandemic era—impact on energy consumption and costs, Energies 17 (4) (2024) 855.

[5] S. Dora, K.M. Mini, Performance assessment of capric acid-ethyl alcohol/expanded vermiculite phase change material incorporated cement mortar for thermal insulation in buildings, J. Energy Storage 72 (2023) 108550, https://doi.org/10.1016/j.est.2023.108550.

[6] D. D'Agostino, M. D'Auria, F. Minelli, F. Minichiello, in: J.R. Littlewood, L. Jain, R.J. Howlett (Eds.), *Multi-criteria Decision-Making For Thermal Insulation Of an Existing Office Building Considering Environmental, Energy, and Economic Performance*, in *Sustainability In Energy And Buildings 2023*, Springer Nature Singapore, Singapore, 2024, pp. 167–177.

[7] M. Foruzan Nia, S.A. Gandjalikhan Nassab, A.B. Ansari, Transient numerical simulation of multiple pane windows filling with radiating gas, Int. Commun. Heat Mass Tran. 108 (2019) 104291, https://doi.org/10.1016/j.icheatmasstransfer.2019.104291.

[8] M.S. Chandra, K. Nandapala, G. Priyadarshana, R.U. Halwatura, Developing a durable thermally insulated roof slab system using bamboo insulation panels. International Journal of Energy and Environmental Engineering 10 (4) (2019) 511–522, https://doi.org/10.1007/s40095-019-0308-x.

[9] D.W. Yarbrough, *12-Reflective Materials and Radiant Barriers for Insulation in Buildings*, in *Materials For Energy Efficiency And Thermal Comfort in Buildings, M.R. Hall*, Woodhead Publishing, 2010, pp. 305–318.

[10] M.T. Araji, A.M. Elmalky, M.G. Yao, Experimental validation of ventilated double-skin façades aided by neural networks and thermal modelling for heating demand reduction, Build. Environ. 256 (2024) 111500, https://doi.org/10.1016/j.buildenv.2024.111500.

[11] D. D'Agostino, D. Faiella, E. Febbraro, E. Mele, F. Minichiello, J. Trimarco, Steel exoskeletons for integrated seismic/energy retrofit of existing buildings - general framework and case study, J. Build. Eng. 83 (2024) 108413, https://doi.org/10.1016/j.jobe.2023.108413.

[12] S.K. Akin, M. AlptekİN, Examining the performance of thermal insulation materials used in buildings for noise insulation, Case Stud. Therm. Eng. 51 (2023) 103556, https://doi.org/10.1016/j.csite.2023.103556.

[13] F. Afsharpanah, S.S. Mousavi Ajarostaghi, M. Arıcı, Parametric study of phase change time reduction in a shell-and-tube ice storage system with anchor-type fin design, Int. Commun. Heat Mass Tran. 137 (2022) 106281, https://doi.org/10.1016/j.icheatmasstransfer.2022.106281.

[14] F. Afsharpanah, K. Pakzad, S.S. Mousavi Ajarostaghi, M. Arıcı, Assessment of the charging performance in a cold thermal energy storage container with two rows of serpentine tubes and extended surfaces, J. Energy Storage 51 (2022) 104464, https://doi.org/10.1016/j.est.2022.104464.

[15] H. Jouhara, J. Yang, Energy efficient HVAC systems, Energy Build. 179 (2018) 83–85, https://doi.org/10.1016/j.enbuild.2018.09.001.

[16] D. D'Agostino, F. Minichiello, F. Petito, C. Renno, A. Valentino, Retrofit strategies to obtain a NZEB using low enthalpy geothermal energy systems, Energy 239 (2022) 122307, https://doi.org/10.1016/j.energy.2021.122307.

[17] V. Akbari, M. Naghashzadegan, R. Kouhikamali, F. Afsharpanah, W. Yaïci, Multi-objective optimization of a small horizontal-Axis wind turbine blade for generating the maximum startup torque at low wind speeds, Machines 10 (9) (2022) 785, https://doi.org/10.3390/machines10090785.

[18] B.P. Jelle, S.E. Kalnæs, et al., Chapter 3-phase change materials for application in energy-efficient buildings, in cost-effective energy efficient building retrofitting, F, Pacheco Torgal. (2017) 57–118 Woodhead Publishing.

[19] F. Afsharpanah, K. Pakzad, S.S. Mousavi Ajarostaghi, S. Poncet, K. Sedighi, Accelerating the charging process in a shell and dual coil ice storage unit equipped with connecting plates, Int. J. Energy Res. 46 (6) (2022) 7460–7478, https://doi.org/10.1002/er.7654.

[20] H.A. Amiri, F. Afsharpanah, S. Moshafi, S. Asiaei, Thermal management of an asymmetrical wavy microchannel heat sink via Ag/water nanofluid, Case Stud. Therm. Eng. 53 (2024) 103857, https://doi.org/10.1016/j.csite.2023.103857.

[21] F. Afsharpanah, M. Izadi, F.A. Hamedani, S.S. Mousavi Ajarostaghi, W. Yaïci, Solidification of nano-enhanced PCM-porous composites in a cylindrical cold thermal energy storage enclosure, Case Stud. Therm. Eng. 39 (2022) 102421, https://doi.org/10.1016/j.csite.2022.102421.

[22] N. Sayoud, A. Laouer, N. Brihi, M. Teggar, M. Arıcı, Melting process enhancement in double pipe storage with multiple latent heat storage materials and oriented fins, J. Energy Storage 85 (2024) 111095, https://doi.org/10.1016/j.est.2024.111095.

[23] F. Afsharpanah, S.S. Mousavi Ajarostaghi, F. Akbarzadeh Hamedani, M. Saffari Pour, Compound heat transfer augmentation of a shell-and-coil ice storage unit with metal-oxide nano additives and connecting plates, Nanomaterials 12 (6) (2022) 1010, https://doi.org/10.3390/nano12061010.

[24] F. Afsharpanah, G. Cheraghian, F. Akbarzadeh Hamedani, E. Shokri, S.S. Mousavi Ajarostaghi, Utilization of carbon-based Nanomaterials and plate-fin Networks in a cold PCM Container with Application in air Conditioning of buildings, Nanomaterials 12 (11) (2022) 1927, https://doi.org/10.3390/nano12111927.

[25] X. Yu, R. Jiang, Z. Li, G. Qian, B. Wang, L. Wang, R. Huang, Synergistic improvement of melting rate and heat storage capacity by a rotation-based method for shell-and-tube latent thermal energy storage, Appl. Therm. Eng. 219 (2023) 119480, https://doi.org/10.1016/j.applthermaleng.2022.119480.

[26] Q. Al-Yasiri, M. Szabó, Incorporation of phase change materials into building envelope for thermal comfort and energy saving: a comprehensive analysis, J.

Build. Eng. 36 (2021) 102122, https://doi.org/10.1016/j.jobe.2020.102122.
[27] M. Hamdani, S.M.E.A. Bekkouche, S. Al-Saadi, M.K. Cherier, R. Djeffal, M. Zaiani, Judicious method of integrating phase change materials into a building envelope under Saharan climate, Int. J. Energy Res. 45 (12) (2021) 18048–18065, https://doi.org/10.1002/er.6951.
[28] M.N. Islam, D.H. Ahmed, Delaying the temperature fluctuations through PCM integrated building walls—room conditions, PCM placement, and temperature of the heat sources, Energy Storage 3 (5) (2021), https://doi.org/10.1002/est2.245.
[29] S. Dardouri, S. Mankai, M.M. Almoneef, M. Mbarek, J. Sghaier, Energy performance based optimization of building envelope containing PCM combined with insulation considering various configurations, Energy Rep. 10 (2023) 895–909, https://doi.org/10.1016/j.egyr.2023.07.050.
[30] A. Ahmad, S.A. Memon, A novel method to evaluate phase change materials' impact on buildings' energy, economic, and environmental performance via controlled natural ventilation, Appl. Energy 353 (2024) 122033, https://doi.org/10.1016/j.apenergy.2023.122033.
[31] S. Zhou, A.G. Razaqpur, CFD modeling and experimental validation of the thermal performance of a novel dynamic PCM Trombe wall: Comparison with the companion static wall with and without PCM, Appl. Energy 353 (2024) 121985, https://doi.org/10.1016/j.apenergy.2023.121985.
[32] A.G. Anter, A.A. Sultan, A.A. Hegazi, M.A. El Bouz, Thermal performance and energy saving using phase change materials (PCM) integrated in building walls, J. Energy Storage 67 (2023) 107568, https://doi.org/10.1016/j.est.2023.107568.
[33] Y. Dong, L. Zhang, P. Wang, Z. Liu, X. Su, H. Liao, X. Jiang, Potential evaluation of energy flexibility and energy-saving of PCM-integrated office building walls, J. Build. Eng. 79 (2023) 107857, https://doi.org/10.1016/j.jobe.2023.107857.
[34] M. Izadi, S.F. Taghavi, S.H. Neshat Safavi, F. Afsharpanah, W. Yaïci, Thermal management of shelter building walls by PCM macro-encapsulation in commercial hollow bricks, Case Stud. Therm. Eng. 47 (2023) 103081, https://doi.org/10.1016/j.csite.2023.103081.
[35] O. Arfi, E.H. Mezaache, A. Laouer, Numerical investigation of double layered PCM building envelope during charging cycle for energy saving, Int. Commun. Heat Mass Tran. 144 (2023) 106797, https://doi.org/10.1016/j.icheatmasstransfer.2023.106797.
[36] A.T. Muzhanje, H. Hassan, Microcapsule geometry and nanomaterial enhancement of PCMs (sp07&sp11) for free heating applications, Case Stud. Therm. Eng. 49 (2023) 103327, https://doi.org/10.1016/j.csite.2023.103327.
[37] J. Li, Z. Peng, H. Zhang, H. Tu, X. Sun, F. Peng, C. Jiang, Study on the heat transfer of a concrete wall outfitted with phase change materials, Case Stud. Therm. Eng. 51 (2023) 103520, https://doi.org/10.1016/j.csite.2023.103520.
[38] S.-G. Jeong, D. Seo, S. Choi, S. Kim, Thermal and energy performance evaluation of a dry floor heating system based on hybrid heat storage aggregates for field application, Appl. Therm. Eng. 236 (2024) 121596, https://doi.org/10.1016/j.applthermaleng.2023.121596.
[39] T.L. Bergman, A.S. Lavine, F.P. Incropera, D.P. DeWitt, Fundamentals of Heat and Mass Transfer, 8th ed., WileyPlace, Hoboken, New Jersey, USA, 2020 ISBN: 978-1119722489.
[40] RubithermTechnologiesGmbH, PCM RT-LINE (2023) 2023. https://www.rubitherm.eu/en/productcategory/organische-pcm-rt.
[41] T. Silva, R. Vicente, C. Amaral, A. Figueiredo, Thermal performance of a window shutter containing PCM: numerical validation and experimental analysis, Appl. Energy 179 (2016) 64–84, https://doi.org/10.1016/j.apenergy.2016.06.126.
[42] E. Tunçbilek, M. Arıcı, S. Bouadila, S. Wonorahardjo, Seasonal and annual performance analysis of PCM-integrated building brick under the climatic conditions of Marmara region, J. Therm. Anal. Calorim. 141 (1) (2020) 613–624, https://doi.org/10.1007/s10973-020-09320-8.
[43] Z.a. Liu, J. Hou, D. Wei, X. Meng, B.J. Dewancker, Thermal performance analysis of lightweight building walls in different directions integrated with phase change materials (PCM), Case Stud. Therm. Eng. 40 (2022) 102536, https://doi.org/10.1016/j.csite.2022.102536.
[44] Y.A. Cengel, A. Ghajar, Heat and mass transfer (a practical approach, SI version), McGraw-670 Hill Educ. 671 (52) (2011) 964.
[45] A. Hasan, K.A. Al-Sallal, H. Alnoman, Y. Rashid, S. Abdelbaqi, Effect of phase change materials (PCMs) integrated into a concrete block on heat gain prevention in a hot climate, Sustainability 8 (10) (2016) 1009.

Nomenclature

C_m: Mushy zone constant [kg/m^3·s]
C_p: Specific thermal capacity [J/kg·K]
e: Enthalpy [kJ/kg]
h: Convective heat transfer coefficient [W/m^2·K]
k: Thermal conductivity [W/m·K]
n: Cartesian directions (*x, y, z*)
P: Pressure [Pa]
p: Period [s]
S: Wind speed [m/s]
T: Temperature [K or °C]
t: Time [s]
V: Velocity vector field [m/s]
W: Energy consumption per unit of area [J/m^2 or W·hr/m^2]
$\dot{W}$: Heat flux [W/m^2]

Greek Symbols
β: Thermal expansion coefficient [1/K]
μ: Dynamic viscosity [Pa·s]
ρ: Density [kg/m^3]
φ: Solid fraction

Subscripts
Avg: Average
c: Cold
f: Floor
h: Hot
liquid: Liquidus
r: Roof
solid: Solidus
surf: Surface
w: Wall
0: Reference
∞: Free stream

Abbreviations
CFD: Computational fluid dynamics
PCM: Phase change material